Ultra Low-Power Wireless Sensor Node for Structural Health Monitoring

Dao Zhou

Thesis submitted to the faculty of the
Virginia Polytechnic Institute and State University
in partial fulfillment of the requirements for the degree of

Master of Science
In
Electrical Engineering

Dong S. Ha, Chair
Daniel J. Inman
Patrick Schaumont

January 18, 2009
Blacksburg, VA

Keywords: Structural Health Monitoring, wireless sensor, Impedance-based method, low power, temperature compensation

Ultra Low-Power Wireless Sensor Node for Structural Health Monitoring

Dao Zhou

(ABSTRACT)

Structural Health Monitoring (SHM) is the technology of monitoring and assessing the condition of aerospace, civil, and mechanical infrastructures using a sensing system integrated into the structure. Among variety of SHM approaches, impedance-based method is efficient for local damage detection. This thesis focuses on system level concerns for impedance-based SHM. Two essential requirements are reached in the thesis: reduction of power consumption of wireless SHM sensor, and compensation of temperature dependency on impedance. The proposed design minimizes power by employing on-board signal processing, and by eliminating power hungry components such as ADC and DAC. The prototype implemented with MSP430 micro controller is verified to be able to handle SHM operation and wireless communication with extremely low-power: 0.15 mW during the inactive mode and 18 mW during the active mode. Each SHM operation takes about 13 seconds to consume 236 mJ. When our ASN-2 operates once in every four hours, it can run for about 2.5 years with two AAA-size batteries. To compensate for temperature change, we proposed an algorithm to select a small subset of baseline profiles for some critical temperatures and to estimate the baseline profile for a given ambient temperature through interpolation. Experimental results show that our method reduces the number of baseline profiles to be stored by 45%, and estimates the baseline profile of a given temperature accurately.

To my parents

Thank you for your endless support and love in my life

Acknowledgement

I would like to express my deepest appreciation to my advisor, Dr. Dong S. Ha for providing excellent support and guidance though my study, research, and writing. His advice and motivation will always lead me through my career life. It was a precious experience to working with him as a member of Virginia Tech VLSI for Telecommunication Lab.

I am also thankful to Dr. Daniel J. Inman at Center for Intelligent Material System and Structures in Mechanical Engineering at Virginia Tech. His technical and financial support, as while as his kind personality made my study enjoyable. I appreciate Dr. Patrick Schaumont for serving on my advisory committee and for being very accommodating and understanding.

In addition, I want to thank the Association of American Railway, Physical Acoustics Corporation, under a contract through the National Institute of Standard and Technology, and Extreme Diagnostics, Inc, under a contract through NASA (SB102), for their financial support of this research.

I would like to thank my fellow colleagues in VTVT lab, including Jeongki Kim, Na Kong, Jihoon Jeong, Jinsik Yun, Vipul Chawla, Hung-Chih Lin, Travis Cochran, Justin Cartwright and Yumi Lim. It was a great pleasure working with them in the past two years. I wish them all great success in their research and future career.

I would like to give a special thanks to my parents, Damai Zhou and Guiru Liu. Their constant and endless love, support, encouragement and advice play a crucial role in everything I do.

Thank to all my friends in Blacksburg. They made the life in this small town lively and enjoyable.

Table of Contents

List of Figures

List of Tables

Chapter 1: Introduction

Structural Health Monitoring (SHM) is the science and technology of monitoring and assessing the condition of aerospace, civil, and mechanical infrastructures using a sensing system integrated into the structure. SHM is capable of detecting, locating, and quantifying various types of damage such as cracks, holes, corrosion, collusions, delimitations, and loose joints, and can be applied to various kinds of infrastructures such as buildings, railroads, windmills, bridges, and aircrafts. A variety of approaches for SHM have been proposed and investigated, and an impedance method based on piezoelectric wafers, such as PZT(Lead Zirconate Titanate), is proven to be effective for in situ local damage detection. In spite of its effectiveness, the PZT based SHM approach still has not been deployed in large-scale applications.

There are two major concerns that block the impedance-based SHM to be widely deployed in industry. Firstly, conventional impedance-based health monitoring employs expensive equipment such as impedance analyzer, which provides excellent performance but at the cost of large physical size, high power consumption and high expense of installation and maintenance. Thus, low power, self-contained sensor nodes, possibly with simple wireless access, are preferred to push the impedance-based health monitoring into real world application.

Secondly, the impedance of a structure can be significantly changed due to variations other than damage, such as loading, boundary conditions, and temperature changes. These factors need to be carefully considered when an impedance-based monitoring system is employed for in-situ applications, especially in harsh environment.

The motivation of this thesis is to develop a SHM system to mitigate the above issues. Introducing wireless communication into SHM substantially reduces the cost of power cable layouts, especially for those applications which need sensors to be

distributed in a large scale. However, to ensure the wireless sensors running independently without increasing the labor for maintenance or battery replacement, a reliable SHM system with low power consumption is essential. Since temperature variation is one of the critical factors that affect the reliability, compensation should be included by studying the effect of temperature change and sensing the ambient temperature.

Based on above considerations, this thesis presents a development of a low-power, temperature compensating wireless sensor node for SHM purpose. Two chapters are included in this thesis to present the complete design.

Chapter 2 demonstrates a wireless sensor node design emphasizing reducing the power consumption of a SHM system. The proposed design minimizes power by employing on-board signal processing, and by eliminating power hungry components such as ADC and DAC. The prototype implemented with MSP430 micro controller is shown to be able to handle SHM operation and wireless communication with extremely low-power.

Chapter 3 discusses a temperature compensation algorithm based on baseline selection and interpolation. The compensation algorithm is design to be used for the low power microcontroller as mentioned in Chapter 2. Consumption of small memory capacity and ability to accurately estimate the baseline profile of a given temperature are explained in this chapter.

Chapter 4 concludes the work included in this thesis. Possible applications and future works are discussed in this chapter.

Chapter 2: Ultra Low-power Active Wireless Structure Health Monitoring Node

*This Chapter is primarily derived from: Zhou, D., Ha, D. S., Inman, D., J., (2010) "Ultra Low-Power Wireless Sensor for Structural Health Monitoring", *Journal of Smart Structures and Systems*, (Accepted)

Abstract

Structural Health Monitoring (SHM) is the science and technology of monitoring and assessing the condition of aerospace, civil, and mechanical infrastructures using a sensing system integrated into the structure. Impedance-based SHM measures impedance of a structure using a PZT (Lead Zirconate Titanate) patch. This chapter presents a low-power wireless autonomous and active SHM node called Autonomous SHM Sensor 2 (ASN-2), which is based on the impedance method. In this study, we incorporated three methods to save power. First, entire data processing is performed on-board, which minimizes radio transmission time. Considering that the radio of a wireless sensor node consumes the highest power among all modules, reduction of the transmission time saves substantial power. Second, a rectangular pulse train is used to excite a PZT patch instead of a sinusoidal wave. This eliminates a digital-to-analog converter and reduces the memory space. Third, ASN-2 senses the phase of the response signal instead of the magnitude. Sensing the phase of the signal eliminates an analog-to-digital converter and Fast Fourier Transform operation, which not only saves power, but also enables us to use a low-end low-power processor. Our SHM sensor node ASN-2 is implemented using a TI MSP430 microcontroller evaluation board. A cluster of ASN-2 nodes forms a wireless network. Each node wakes up at a predetermined interval, such as once in four hours, performs an SHM operation, reports the result to the central node wirelessly, and returns to sleep. The power consumption of our ASN-2 is 0.15 mW during the inactive mode and 18 mW during the active mode. Each SHM operation takes about 13 seconds to consume

236 mJ. When our ASN-2 operates once in every four hours, it is estimated to run for about 2.5 years with two AAA-size batteries ignoring the internal battery leakage.

2.1 Introduction

Structural Health Monitoring (SHM) is the science and technology of monitoring and assessing the condition of aerospace, civil, and mechanical infrastructures using a sensing system integrated into the structure. SHM is capable of detecting, locating, and quantifying various types of damage such as cracks, holes, corrosion, collusions, delimitations, and loose joints, and can be applied to various kinds of infrastructures such as buildings, railroads, windmills, bridges, and aircrafts. A variety of approaches for SHM have been proposed and investigated. The impedance method based on using piezoelectric wafers, such as PZT (Lead Zirconate Titanate), is proven to be effective for in situ local damage detection. Unlike passive sensing methods, the impedance-based method combines sensing with actuation, which sweeps a certain frequency range to measure the impedance profile of a structure. In spite of its effectiveness, the PZT based SHM approach still has not been deployed in large-scale applications.

Major roadblocks for field deployment include high hardware complexity and high installation cost (including laying out cables for power supply and data collection). High hardware complexity is attributed to the need for generation of an excitation signal, collection of the response signal, and processing of the collected data. Existing SHM prototypes rely on expensive instruments and/or high-speed DSP chips. High hardware complexity incurs high power consumption, a large form factor, and high cost. Among them, power consumption is especially problematic for many SHM applications, where line power is unavailable (such as a blade of a windmill) or laying out cables is undesirable (such as wings of an airplane). Even if line power is available (such as a bridge with street lights), drawing a cable to a sensor node is costly. Ideally, an SHM node/system dissipates extremely low power, so that it can run on a small-size battery for several years or run on energy harvested from ambient sources, such as solar, thermal, or

vibration. In such a case, wireless transmission of the SHM data to the host computer is essential to remove wires from the node to the host.

In this chapter, we present a low-power wireless autonomous and active SHM node called ASN-2, which is based on the impedance method. Our system incorporates three methods for reduction of power, and experimental results show our system is highly efficient in power. It should be noted that the focus of the chapter is low-power design of our SHM system, not wireless networking nor the impedance method itself. The chapter is organized as follows: Section 2 provides background and preliminaries necessary to understand our work. We also review a few existing SHM systems relevant to our system. Section 3 presents three power saving methods, which are incorporated into ASN-2. Section 4 describes details about ASN-2 such as its architecture, system operation, temperature compensation, and wireless networking. Section 5 presents experimental results including a power dissipation profile. Finally, we conclude the chapter in Section 6.

2.2 Preliminaries and Literature Review

We describe the impedance-based method and review a few relevant SHM systems in this section. Figure 2.1 shows a model of an impedance-based SHM, in which an electrical sinusoid signal $V(\omega)$ actuates the PZT. The PZT transforms the electrical signal into the mechanical strain. The admittance of the piezoelectric patch $Y(\omega)$ is a combined function of the impedance of the PZT actuator $Z_a(\omega)$ and that of the host structure $Z(\omega)$ is given by

$$Y(\omega) = j\omega a(\varepsilon_{33}^{T}(1-\delta) - \frac{Z(\omega)}{Z(\omega)+Z_a(\omega)} d_{3x}^{2} Y_{XX}^{E}) \tag{2.1}$$

where a, d_{3x}^{2}, δ, Y_{XX}^{E} and ε_{33}^{T} are the geometry constant, the piezoelectric coupling constant, the dielectric loss tangent, Young's modulus, and the complex dielectric constant of the PZT at zero stress, respectively [7]. The first term in the equation is the

capacitive admittance of a free piezoelectric patch, and the second one is the result of the electromechanical interaction of the piezoelectric patch with the host structure [12].

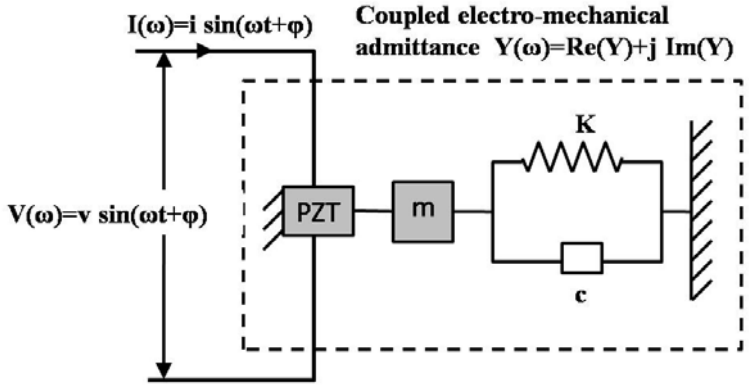

Figure 2.1: Model of an impedance-based SHM

Previous studies indicate that the real part of the admittance given in (2.1) is more sensitive to damage of the structure, while the imaginary part to the temperature variation [8]. Hence, it is desirable for an SHM system to be sensitive to the real part and to suppress the side effect caused by the imaginary part. Krishnamurthy et al. showed through experiments that the magnitude of impedance peaks shrink as the temperature increases, while peaks of the imaginary part shift towards a lower frequency [4]. Consequently, an impedance-based SHM requires a mechanism to compensate the temperature variation.

Conventional impedance-based SHM methods rely on impedance analyzers. Such instruments provide high precision measurements for a large frequency range, but they are bulky and, hence, not suitable for in-situ applications. Analog Device, Inc. introduced an impedance analyzer chip AD5933, which dissipates about 30 mW. The chip includes a digital-to-analog converter to generate an excitation signal up to 100 kHz, a 12-bit analog-to-digital converter, and supports on-chip Fast Fourier Transform (FFT) operation. Park et al. integrated this chip with a microcontroller ATMega128 and an XBee wireless transceiver [9]-[11]. They showed that the system could be applicable for various SHM

applications, but high-power consumption is a major issue. Researchers from Los Alamos National Lab have worked on a series of wireless SHM sensor systems embedded with Analog Device's impedance analyzer chips AD5933 for years and developed the third generation of the sensor system called Wireless Impedance Device (WID-3) in 2009 [6],[5],[13]. The power consumption of WID-3 is around 70 mW during measurement and wireless transmission [1],[14]. Our team also developed an impedance-based SHM system using a Texas Instrument DSP evaluation board. The SHM system verifies effectiveness of rectangular pulse trains as the excitation signal, but consumes about 800 mW due to unnecessary chips and components embedded on the evaluation board [2],[3].

2.3 Proposed Method for Low-power System Design

In this section, we present three methods employed for low-power design of our wireless SHM sensor node. The first method is on-board data processing to reduce the radio transmission time, which substantially reduces the power dissipated by the radio. The second method is elimination of a digital-to-analog converter (DAC) for excitation signal generation, and the third one is elimination of an analog-to-digital converter (ADC) for response sensing.

2.3.1 On-board Data Processing

The major source of power consumption for a wireless sensor node is the radio. For example, a microcontroller unit TI MSP430 from Texas Instruments used for our SHM sensor node dissipates 3 mW under a low-power operation mode, while a low-end radio CC2500 from Texas Instruments embedded in the sensor node dissipates 65[1] mW during transmission. So, it is essential to reduce the radio transmission time for a low-power wireless SHM sensor node. We adopt an on-board data processing approach for our SHM sensor node, which processes the data on the board and sends only the final outcome (healthy or damaged) of the SHM operation to the control center. So, the radio

[1] This value is from the data sheet.

for our sensor node transmits only three bytes of data, including the outcome of the SHM operation and the ambient temperature.

2.3.2 Elimination of DAC for Generation of Excitation Signal

A sinusoidal signal sweeping a certain frequency range is usually used to excite a PZT patch for the impedance method. Generation of a sinusoidal signal usually relies on a DAC. Sampled values of a sinusoidal signal are pre-stored in a memory, and a processor reads the pre-stored data and applies it to a DAC to generate the corresponding analog signal. This method is straightforward, but it requires a DAC and a large memory space for a large-frequency sweeping range.

Our method is to employ a rectangular pulse train rather than a sinusoidal signal. A rectangular pulse train illustrated in Figure 2.2 (a) has the duty cycle of 0.5, and its fundamental frequency (which is given as $1/t_p$, where t_p is the pulse period) sweeps a certain desired frequency range. The Fourier transform of a pulse train with a pulse period t_p and a duty cycle of 0.5 has odd harmonics kf_o, $k=1, 3, 5 \ldots$, where $f_o = 1/t_p$. Figure 2.2 (b) illustrates frequency components of a pulse train with the fundamental frequency ranging from 40 kHz to 50 kHz. The magnitude of the third harmonic is about 33 percent of the fundamental frequency, and the fifth one about 20 percent.

A rectangular pulse train is digital, and hence a processor can directly generate such a signal. Since generation of a rectangular pulse train does not require a DAC, it reduces power consumption of an SHM sensor node. One potential issue is existence of harmonics on the signal. Note that our interest is to detect the difference between the baseline impedance profile and a currently measured one. Since both profiles are under the subject of the same frequency terms, the sensitivity for detecting the difference may not be affected by harmonics. Further, harmonic terms decrease rapidly, and some harmonic terms may be out of the interested frequency range. Our experimental results reveal that use of a rectangular pulse train does not incur any noticeable deterioration of the performance for the impedance method [2].

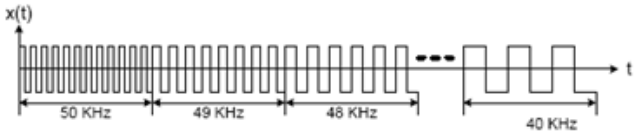

(a) Time domain

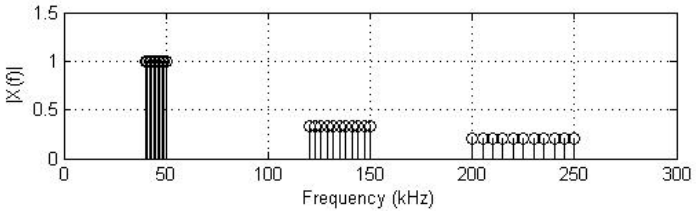

(b) Frequency domain

Figure 2.2: Rectangular pulse train

2.3.3 Elimination of ADC for Sensing of Response Signal

Existing methods such as Analog Device's impedance analyzer chips sample the response signal using an ADC and performs a Fast Fourier Transform (FFT) to extract the impedance component of the frequency. A typical ADC used for an SHM system consumes large power, possibly next to a radio and a processor, and FFT is also computationally intensive to increase power dissipation. Our method is to eliminate an ADC and the FFT operation by sensing the phase, not the magnitude, of the response signal.

The electrical admittance is expressed as $Y(jf) = G(f) + jB(f)$, where $G(f)$ and $B(f)$ are conductance and susceptance terms, respectively. It is known that the conductance term of a PZT patch is more sensitive to damage [7]. Let $G_{base}(f)$ denote the baseline conductance obtained from a healthy structure and $G_{SUT}(f)$ be the conductance of a structure under test (SUT). The difference of the two conductance terms $G_{base}(f) - G_{SUT}(f)$ is used for existing impedance-based SHM systems to detect damage. Our earlier work showed that

$$G_{base}(f) - G_{SUT}(f) \approx C \sin[\phi_{base}(f) - \phi_{SUT}(f)] \tag{2.2}$$

where C is a constant, assuming all parameters other than the impedance in expression (1) are constant, and $\phi_{base}(f)$ and $\phi_{SUT}(f)$ are the phase of the baseline admittance and the SUT admittance, respectively. Expression (2.2) suggests that difference of the phases, instead of the conductance *G(f)*'s, can be sensed for the impedance method.

The phase of an admittance $\phi(f)$ for a frequency f can be expressed as in (3), where $T_d(f)$ is the time difference between the voltage and the current:

$$\phi(f) = 2\pi f \times T_d(f) \tag{2.3}$$

When both the voltage and current are represented as binary signals, the phase difference of the two signals is obtained using an exclusive-OR (XOR) operation as illustrated in Figure 2.3. A processor can measure the time delay by sampling the output of the XOR operation at a system clock frequency, where the system clock frequency is typically much higher than the frequency f of the admittance under consideration.

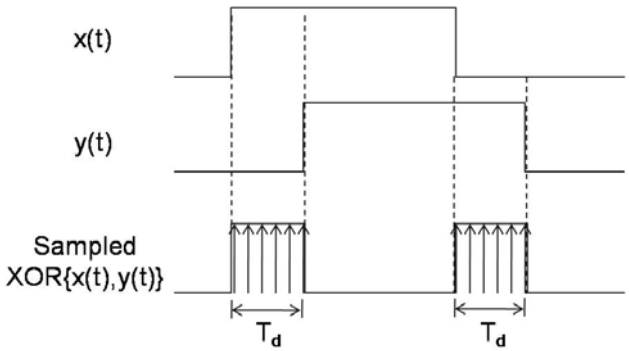

Figure 2.3: Phase difference represented with delay in time domain

Figure 2.4 shows a circuit diagram for a phase measurement. A rectangular pulse train $V_{in}(t)$ is applied to the PZT attached to the structure. The output of the operational amplifier (opamp) shows the current waveform through the PZT, which is delayed in time by a certain amount. The reference voltage V_{ref} shifts the DC level of the applied input voltage, and it is set to 1/2 of peak-to-peak voltage of input signal $V_{in}(t)$. The second opamp is a comparator, which shapes the current waveform into digital. The XOR gate detects the difference between the input voltage and the current through the PZT.

Figure 2.4 shows a simplified circuit diagram for a phase measurement. A rectangular pulse train $V_{in}(t)$ is buffered by an operational amplifier (opamp) and applied to the PZT attached to the structure. The output of opamp OP3 is the current through the PZT, which is delayed in time by a certain amount. The reference voltage V_{ref} shifts the DC level of the applied input voltage, and it is set to one half of the peak-to-peak voltage of input signal V_{in}(t). OP4 is a comparator, which shapes the current waveform into digital. The XOR gate detects the difference between the input voltage and the current through the PZT. OP1 is necessary to drives a highly capacitive PZT, and OP2 is added to delay the excitation signal by the same amount as OP1.

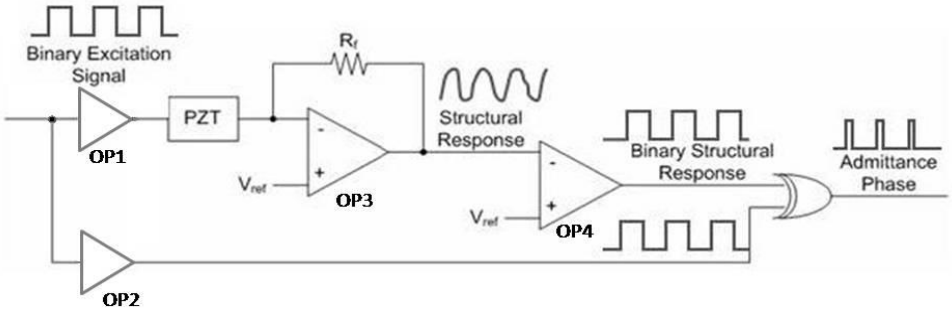

Figure 2.4: Phase measurement circuit

2.4 System Development of Wireless Autonomous Sensor

We developed an autonomous SHM node called ASN-2, which is an improved version of our earlier one reported in [2]. The major focus of ASN-2 is low-power design of an SHM system based on the impedance method, not wireless networking nor the impedance method itself. ASN-2 incorporates the low-power design methods described in Section 3 and was developed using a low-power microcontroller evaluation board. We describe ASN-2 in this section including its architecture, system operation, damage metric, temperature compensation, and wireless networking.

2.4.1 Architecture and Prototype

ASN-2 was developed using a TI MSP430 low-power microcontroller from Texas Instruments, which contains an embedded temperature sensor. The maximum clock

frequency of MSP430 is 16 MHz. We chose a low clock frequency of 1.2 MHz to save power, but the frequency is high enough for generation of a pulse train in our desired frequency range. The microcontroller can be programmed to operate in several modes with different levels of power consumption. It consumes about 3 mW in the active mode for ANS-2 and only 3 μW in the sleep mode.

The microcontroller evaluation board ez430-RF2500 used for ASN-2 has a radio called CC2500 operating at 2.4 GHz. The data rate of the radio is programmable and can reach up to 500 kbps, and its coverage is less than 20 meters for an outdoor environment. Also, the radio can be configured to operate in the active mode or sleep mode. It consumes 65 mW during transmission, and as low as 1.2 uW in the sleep mode, The architecture of our SHM sensor node based on TI MSP430 microcontrollers is shown in Figure 2.5.

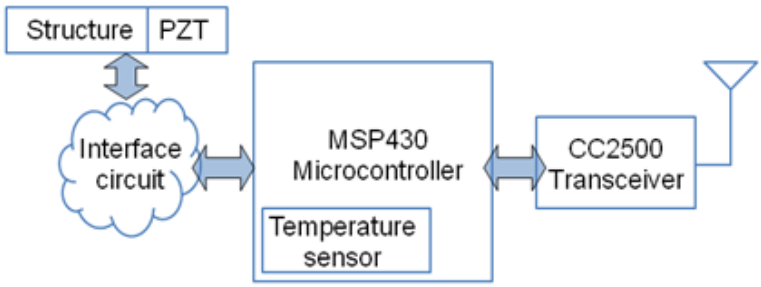

Figure 2.5: Architecture of our SHM sensor node ANS-2

A prototype for ASN-2 is shown in Figure 2.6. The top part is the interface analog circuit, and the bottom part is the evaluation board and two AAA-size batteries. The size of the prototype is 4.5 cm×7 cm× 3 cm, and it runs on two AAA-size batteries.

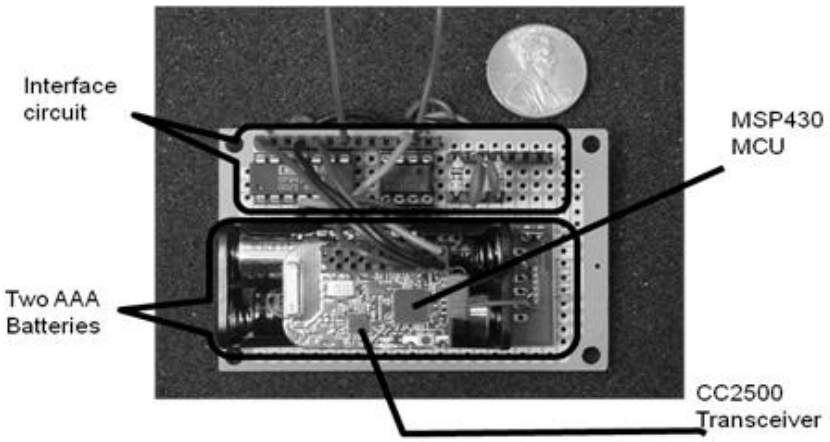

Figure 2.6: Prototype of ASN-2 developed using a TI MSP430 evaluation board

2.4.2 System Operation

Figure 2.7 shows the system operation of ASN-2. The microcontroller sweeps a user specified frequency range and measures the phase profile of a baseline or SUT for the frequency range. It repeats the same operation four times and takes the average value to obtain the phase profile. Each SHM operation including four repeated measurements and processing of the response data, takes about 13 seconds for a frequency range from 12 KHz to 35 KHz. After an SHM operation, ASN-2 goes into the sleep mode for a predetermined time period controlled by an internal timer. During the sleep mode, most components such as the CPU, opamps, and the built-in ADC (used to sample temperature sensor values for ASN-2) are turned off, and some other components such as the timer and the radio are set to a lower clock frequency or the sleep mode.

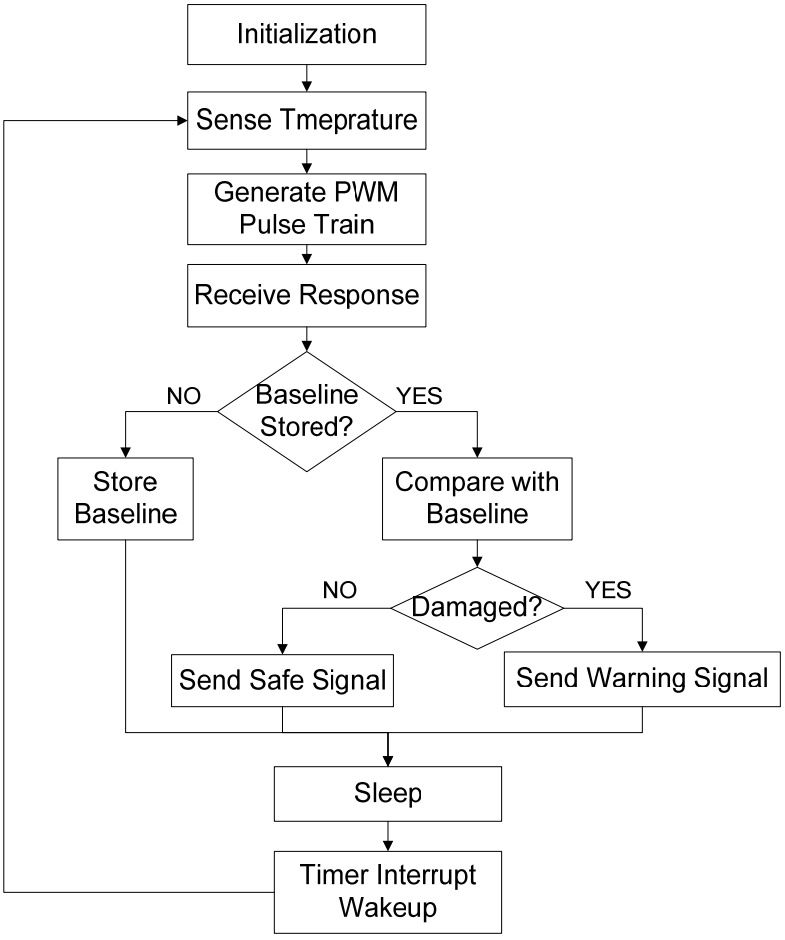

Figure 2.7: system operation flow of ASN-2

2.4.3 Damage Metric

The damage metric (DM) for our system is defined as a normalized absolute sum of differences between the phase profiles of the baseline and of the SUT given by

$$\mathrm{DM} = \frac{\sum_{f_i=f_l}^{f_h} \left| \phi_{base}(f_i) - \phi_{SUT}(f_i) \right|}{M(f_l, f_h)} \tag{2.4}$$

where $M(f_l, f_h)$ is the number of frequency points from the lowest frequency f_l to the highest frequency f_h. The DM of a SUT is compared against a threshold value, whose value may be set based on field experience. If the DM is lower than the threshold value, the SUT is considered healthy. Otherwise, it is damaged. It is important to note that fixed-point calculations without involving multiplications or division are sufficient for

Expression (2.4) provided $M(f_l, f_h)$ is set to power of 2. So, a simple fixed-point processor, rather than a floating-point processor, can be used for our SHM system to save power. Adoption of a more sophisticated DM is possible for ASN-2 to improve the SHM performance, but it is not the objective of ASN-2.

2.4.4 Wireless Networking

The radio included in ASN-2 is a low-power wireless transceiver CC2500 developed by Texas Instruments. It operates in the band of 2400 MHz to 2483.5 MHz with power dissipation of 65 mW during transmission. The maximum number of sensor nodes supported by current prototype of ASN-2 is ten, and the maximum communication distance between a node and a control center is 10 meters indoors.

A network protocol SimplicTI developed by Texas Instruments targets low-power wireless sensor networks and is adopted for ASN-2. There are three major layers defined for the protocol, the data link/PHY layer, the network layer, and the application layer. ASN-2 adopts a star network topology and a token-based algorithm to avoid conflicts. The control center node assigns a token with a sensor node ID number, and the sensor node with the matching ID number grabs the token, synchronizes its clock with that of the control center, and transmits the data. The data is three bytes long, including the outcome of the SHM operation and the ambient temperature. The transmission data rate is set to 250 kbps for ASN-2, and transmission of one message takes about 30 msec.

2.5 Experimental Results

In this section, we present experimental results and a power dissipation profile of ASN-2 during an SHM operation.

2.5.1 Test Structure and Environment

The test structure for our experiments is an aluminum beam with a PZT patch attached at one end. The test structure is hung in free air at the room temperature of around 20° C. A pair of identical magnets are placed on both sides of the beam at a

certain position, and the pressure applied to the structure simulates damage. The size of the test beam and four different positions of the two magnets considered for our experiments are shown in Figure 2.8.

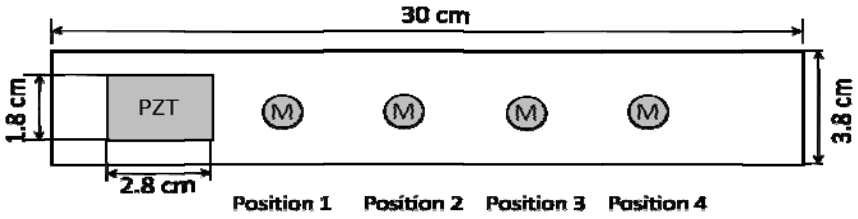

(a) Top view

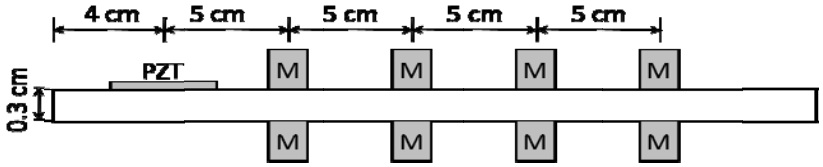

(b) Side view

Figure 2.8: Test structure and position of magnets

To identify a sensitive frequency range of the test beam, we measured the impedance of the healthy beam with an impedance analyzer, Agilent 4294A. The impedance profile of the healthy beam is shown in Figure 2.9. As shown in the figure, the phase of the measured impedance is sensitive in the frequency range from 12 kHz to 35 kHz, and hence the range is set for our experiments.

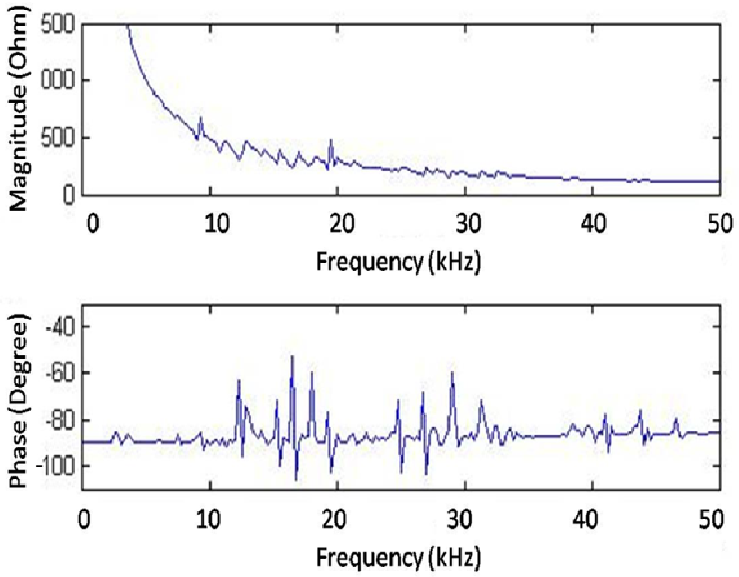

Figure 2.9: Impedance of the healthy structure

2.5.2 SHM Performance

We performed SHM operations with ASN-2, in which the excitation pulse train sweeps from 12 KHz to 35 KHz. Since the phase profile of a SUT changes from one measurement to the next due to noise or other environment changes, we conducted 20 experiments for the baseline and for each damage, i.e., each position of the magnets, and computed the DM values using expression (2.4). Statistical data for the DM values are tabulated in Table I and presented in Figure 2.10.

Table 2-1: DM values for 20 experiments

	Baseline	Position 1	Position 2	Position 3	Position 4
Average	3.4	19.2	16.9	15.6	24.2
Maximum	6.7	22.6	17.6	15.9	25.5
Minimum	0.3	18.1	16.3	15.2	23.1
Standard Deviation	1.72	1.29	0.41	0.23	0.79

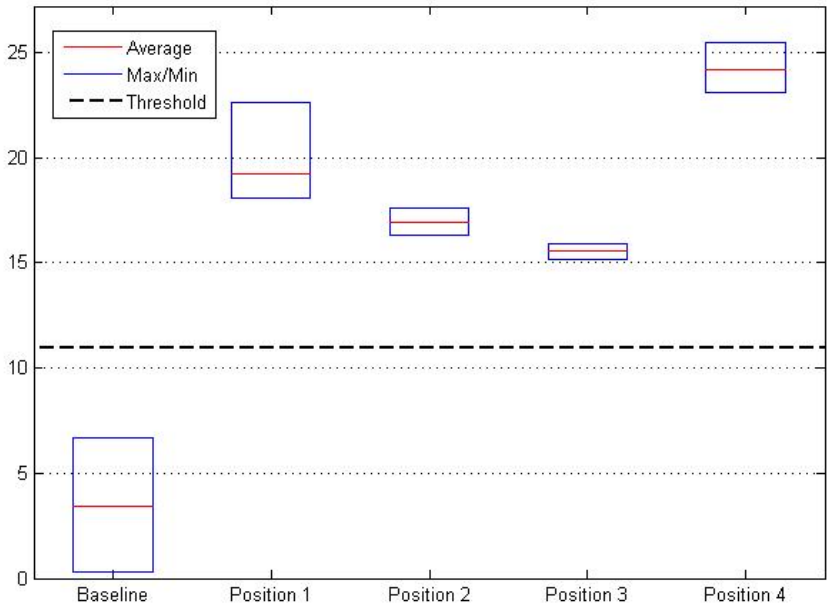

Figure 2.10: Difference of DM values between the baseline and the four damages

The average DM value of the baseline structure is 3.4, while those for damaged structures range from 15.6 to 24.2. The large difference in the averages values of the

baseline and of damaged structures combined with small standard deviations assures detection of damage with high confidence for ASN-2. If the threshold is set between 6.7 and 15.2, ASN-2 does not incur any false alarm for the particular damages, and the dotted line Figure 2.10 indicates the optimal DM value (which is the middle point between 6.7 and 15.2). It should be noted that the DM value decreases from Position 1 to Position 3, but increases sharply at Position 4. The result indicates that the proposed damage metric cannot be used to locate damage.

2.5.3 Power Profile

The supply voltage of two AAA-size batteries remained at constant 3 V during our experiments, and so we measured only the current flowing into ASN-2. The measured current profile over one SHM operation of ASN-2 is shown in Figure 2.11. The current under the inactive mode is about 50 μA to result in 0.15 mW of power consumption. The current increases to an average of 6 mA during the active mode with the radio off, which dissipates 18 mW. The active mode lasts for about 13 seconds to consume 234 mJ of energy. When the radio is turned on at the end of the active mode, the current jumps abruptly to 23 mA to cause 70 mW of power consumption. However, the period lasts for about 30 msec to result in 2.1 mJ of energy consumption.

The supply voltage of two AAA-size batteries remained at constant 3 V during our experiments, and so we measured only the current flowing into ASN-2. The measured current profile over one SHM operation of ASN-2 is shown in Figure 2.11. The current under the inactive mode is about 50 μA resulting in 0.15 mW of power consumption. The current increases to an average of 6 mA during the active mode with the radio off, which dissipates 18 mW. The active mode lasts for about 13 seconds consuming 234 mJ of energy. When the radio is turned on at the end of the active mode, the current jumps abruptly to 23 mA causing 70 mW of power consumption. However, the period lasts for about 30 msec resulting in 2.1 mJ of energy consumption.

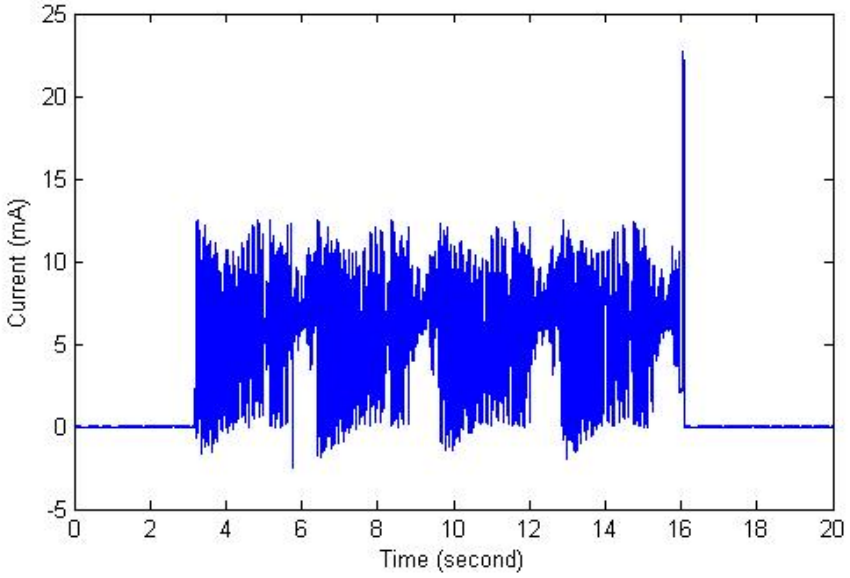

Figure 2.11: Measured current profile during on SHM operation

When ASN-2 operates once in every four hours, the average power consumption is 0.16 mW. Considering the typical capacity of an AAA-size battery is about 1200 mAh, ASN-2 can run for about 2.5 years ignoring the internal battery leakage. It is feasible for ASN-2 to be powered by energy harvested from ambient sources such as solar, thermal, or vibration. We conclude this section by noting that the above power consumption is limited for our experiments. The power consumption of ASN-2 varies widely depending on multiple parameters such as the frequency of SHM operations per a given period, the amount of data to be transmitted, and the topology of the network.

2.6 Conclusion

We presented a low-power wireless autonomous and active SHM node ASN-2, which is based on the impedance method. We incorporated three methods to save power. First, the entire data processing is performed on-board, which minimizes the radio transmission time. Considering the radio of a wireless sensor node consumes the most power, reduction of the transmission time saves substantial power. Second, a rectangular pulse train is used to excite a PZT patch instead of a sinusoidal signal. This eliminates a DAC and reduces the memory space. Third, it senses the phase of the response signal

instead of the magnitude. Sensing the phase of the signal eliminates an ADC and FFT operation, which not only saves power, but also enables us to use a low-end low-power processor. Our SHM sensor node ASN-2 is implemented using a TI MSP430 microcontroller evaluation board. A cluster of ASN-2 nodes forms a wireless network. Each node wakes up at a predetermined interval such as once in four hours, performs an SHM operation, reports the result to the central node wirelessly, and returns to sleep. The power consumption of our ASN-2 is 0.15 mW during the inactive mode and 18 mW during the active mode. Each SHM operation takes about 13 seconds to consume 236 mJ. When our ASN-2 operates once in every four hours, it can run for about 2.5 years with two AAA-size batteries ignoring the internal battery leakage.

References

[1] Farinholt, K.M., Park, G. and Farrar C. R.(2009) "Energy Harvesting and Wireless Energy Transmission for Power SHM Sensor Nodes" *Proc. of 7th International Workshop for Structural Health Monitoring*, Palo Alto, CA, September.

[2] Kim, J., Grisso, B. L., Ha, D. S., and Inman, D. J., (2007). "An All-digital Low-power Structural Health Monitoring System". *IEEE Conference on Technologies for Homeland Security*, 123-8.

[3] Kim, J., Grisso, B. L., Ha, D. S., and Inman, D. J., (2007). "A System-On-Board approach for Impedance-based Structural Health Monitoring" *Proceeding of SPIE,* Vol. 6529, 65290O, San Diego, March.

[4] Krishnamurthy, K., Lalande, F., and Rogers, C. A.,(1996), "Effects of temperature on the electrical impedance of piezoelectric sensors," *Proceeding of SPIE,* Vol. 2717, 302 San Diego, February.

[5] Mascarenas, D. L., Todd, M. D, Park, G. and Farrar, C. R.,(2007), "Development of an impedance-based wireless sensor node for structural health monitoring" *Smart Mater.*

Struct. (16) 6: 2137–2145.

[6] Overly, T.G., Park, G., Farinholt, K.M., Farrar, C.R. (2008), "Development of an extremely compact impedance-based wireless sensing device," *Smart Mat. and Struct.,* (17) 6: 065011.

[7] Park, G., Sohn, H, Farrar, C. R., and Inman, D. J., (2003), "Overview of piezoelectric impedance-based health monitoring and path forward", *The Shock and Vibration Digest,* 35, 451-463.

[8] Park, G., Kabeya, K., Cudney, H. H., and Inman, D. J., (1999), "Impedance-based structural health monitoring for temperature varying applications," *JSME International Journal*, Series A, 42, 249-258.

[9] Park, S., Shin, H., and Yun, C., (2009), "Wireless impedance sensor nodes for functions of structural damage identification and sensor self-diagnosis", *Smart Mater. Struct*., 18- 055001.

[10] Park, S., Yun, C., Inman, D. J., and Park, G., (2008), "Wireless Structural Health Monitoring for Critical Members of Civil Infrastructures Using Piezoelectric Active Sensors", *Proceeding of SPIE,* Vol. 6935, 69350I, San Diego, March.

[11] Park, S., Lee, J., Yun, C., and Inman, D. J., (2008), "Electro-Mechanical Impedance-Based Wireless Structural Health Monitoring Using PCA-Data Compression and k-means Clustering Algorithms", *Journal of Intelligent Material Systems and Structures,* Vol. 19, No. 4, 509-520.

[12] Sun, F. P., Chaudhry, Z., Liang, C. ; Rogers, C. A., (1995) "Truss structure integrity identification using PZT sensor-actuator" *Journal of intelligent material systems and structures,* vol. 6, no1, pp. 134-139 .

[13] Taylor, S.G., Farinholt, K.M., Park, G. and Farrar C. R.(2009) "Impedance-Based Wireless Sensor Node for SHM, Sensor Diagnostics, and Low-Frequency Vibration Data Acquisition" *Proc. of 7th International Workshop for Structural Health Monitoring*, Palo Alto, CA, September.

[14] Taylor, S.G., Farinholt, K.M., Flynn, E. B., Figueiredo, E., Mascarenas, D. L., Park, G., Todd, M.D. and Farrar C. R.(2009) "A Mobile Agent-based Wireless Sensing

Network for SHM Study at the Alamos Canyon Bridge", *Proc. of 7th International Workshop for Structural Health Monitoring*, Palo Alto, CA, September.

[15] Zhou, D., Kim, J. K., Ha D. S., Queensberry, J. D., and Inman, D. J., (2009) "A System Approach for Temperature Dependency of Impedance-Based Structural Health Monitoring". *Proceeding of SPIE,* Vol 7293 72930U, San Diego, March.

[16] Zhou, D., Kim, J. K., Bilé, J.-L. K., Shebi, A. B., Ha, D. S. and Inman, D. J., (2009) "Ultra Low-Power Autonomous Wireless Structural Health Monitoring Node" *Proc. of 7th International Workshop for Structural Health Monitoring*, Palo Alto, CA, September.

Chapter 3: A System Approach for Temperature Dependency of Impedance-based Structural Health Monitoring

*This Chapter is primarily derived from: Zhou, D., Kim, J. K., Ha D. S., Queensberry, J. D., and Inman, D. J., (2009) "A System Approach for Temperature Dependency of Impedance-Based Structural Health Monitoring". *Proceeding of SPIE,* Vol. 7293, 72930U, San Diego, March

Abstract

An impedance-based structural health monitoring (SHM) system employs a piezoelectric patch to excite the structure under test and capture its response. Impedance-based SHM offers several advantages over other methods such as good performance for local damage detection and simple hardware. A major problem for impedance-based SHM is temperature dependency. Specifically, baseline impedance profiles of structures vary as the ambient temperature changes. In this chapter, we propose a new method to compensate the effect of temperature on baseline profiles. Our method is to select a small subset of baseline profiles for some critical temperatures and estimates the baseline profile for a given ambient temperature through interpolation. We incorporated our method into our SHM system and investigated the effectiveness of our method. Our experimental results show that (i) our method reduces the number of baseline profiles to be stored, and (ii) estimates the baseline profile of a given temperature accurately.

3.1 Introduction

An impedance-based structural health monitoring (SHM) system employs a piezoelectric patch to excite the structure under test and to capture its response. Impedance-based SHM offers several advantages over other methods such as good performance for local damage detection and simple hardware. A major problem for an impedance-based SHM is temperature dependency. Specifically, impedance profiles of

structures vary as the ambient temperature changes. In this chapter, we present a different approach, which is to store baseline impedance profiles corresponding to the temperatures in the operating range. A straightforward method is to store impedance profiles of all temperature points in the operating temperature range, but the memory requirement is excessive. An alternative method is to store all the impedance profiles at a host computer and to transmit wirelessly the profile corresponding to the ambient temperature of the SHM system. However, the power consumption for the wireless transmission is a problem for an SHM system operating with a limited power resource. Our method is to select a small subset of baseline impedance profiles for some critical temperatures and estimate the baseline profile for a given ambient temperature through interpolation. To demonstrate effectiveness of our scheme, we incorporated our scheme into our impedance based SHM system.

This chapter is organized as follows. Section 2 describes our impedance-based SHM system, in which the proposed method for temperature compensation is incorporated. Section 3 presents experimental results on impact of temperature to impedance profiles, and Section 4 proposes a method to compensate the temperature dependency. Section 5 concludes the chapter.

3.2 Literature Review

Previous studies show that the real part of the impedance is more sensitive to damage of the structure and less sensitive to the temperature compared with the imaginary part. The magnitude of peaks for the real part shrinks as the temperature increases, while the peaks (which represent its resonant frequencies) for the imaginary part shift to lower frequency band [1]. Several methods were proposed to mitigate the temperature dependency problem. Krishnamurthy et al. suggested a magnitude averaging scheme, which is to calculate the average value of the magnitude assuming a linear relationship between the magnitude and the temperature. [1]. Park et al. investigated a

temperature compensation scheme in the prospective of damage metric correction. The damage metric was adjusted to eliminate the horizontal shift of impedance peaks [1].

3.3 Temperature Effect on Impedance Profiles

Our system measures the phase of the admittance rather than the conductance term. We tested the effect of temperature to phase profiles of the structure and show the results in this section. We use the term impedance profile (instead of phase profile) hereafter.

3.3.1 Experiment Setup

Our test structures, one healthy and one damaged, are two same size aluminum beams shown in Figure 3.1, and a damage was simulated with a drilled hole at the center of a beam. The test structures were hung inside a temperature chamber (Tenney Environmental Chamber 36ST) and connected to our digital SHM system sitting outside of the chamber as shown in Figure 3.2. A computer is connected to the SHM system to collect and display data in real time.

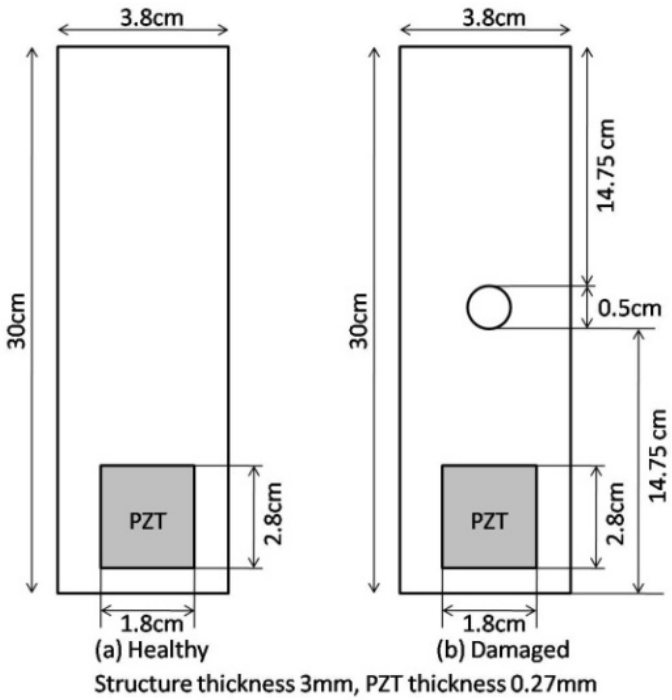

Figure 3.1: Test Aluminum Beams: Healthy and Damaged

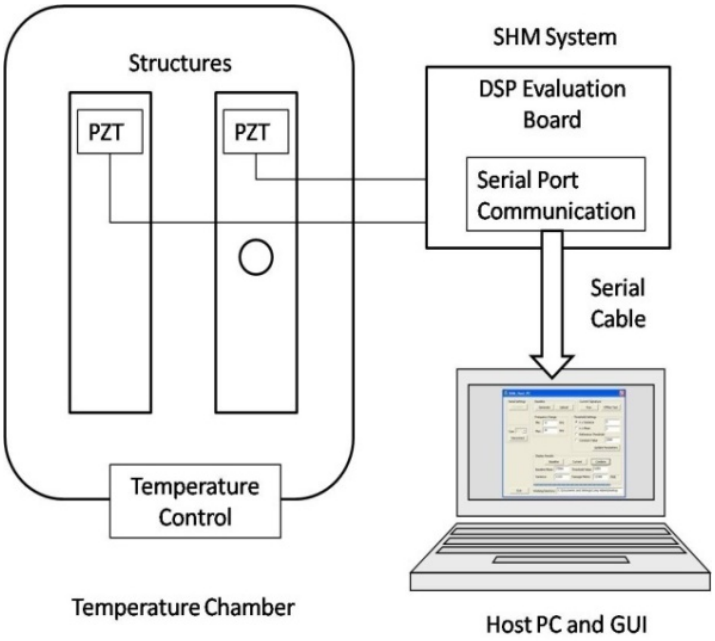

Figure 3.2: Experiment Setup

The temperature range for our experiments was set from -40°C to 80°C with an increment of 10°C, which results in 13 different temperatures for our experiments. The highest temperature was decided by the epoxy used to attach PZT patches, which started to lose its strength significantly beyond 80°C. We identified a frequency range from 12 kHz to 25 kHz using an impedance analyzer (HP 4294A), in which the impedance profiles of both the healthy and the damaged structures have dense peaks. We set the frequency band as the target frequency range for our SHM system. Figure 3.3 shows the impedance profiles of the structures tested by the impedance analyzer at temperature 20°C.

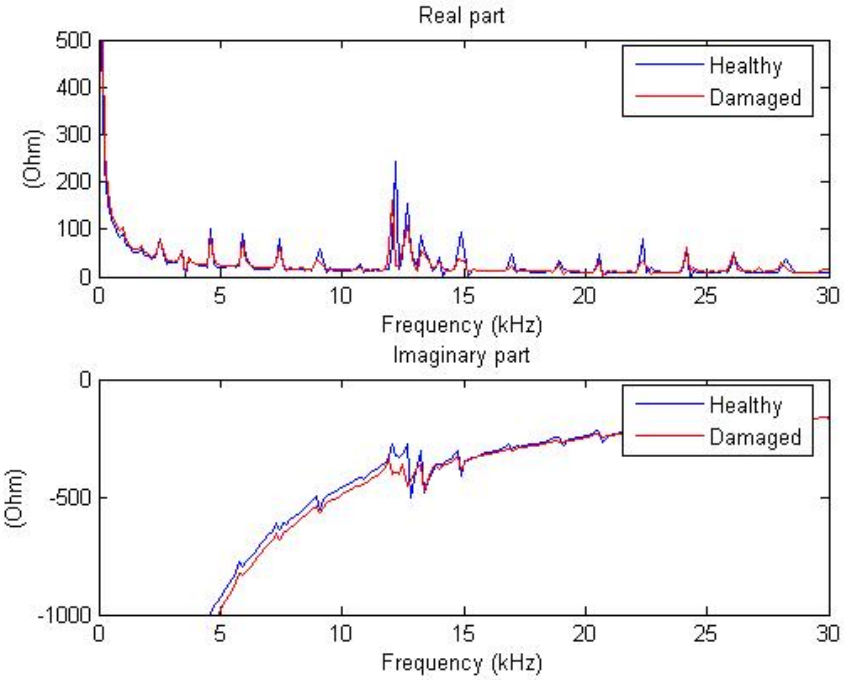

Real part and Imaginary part

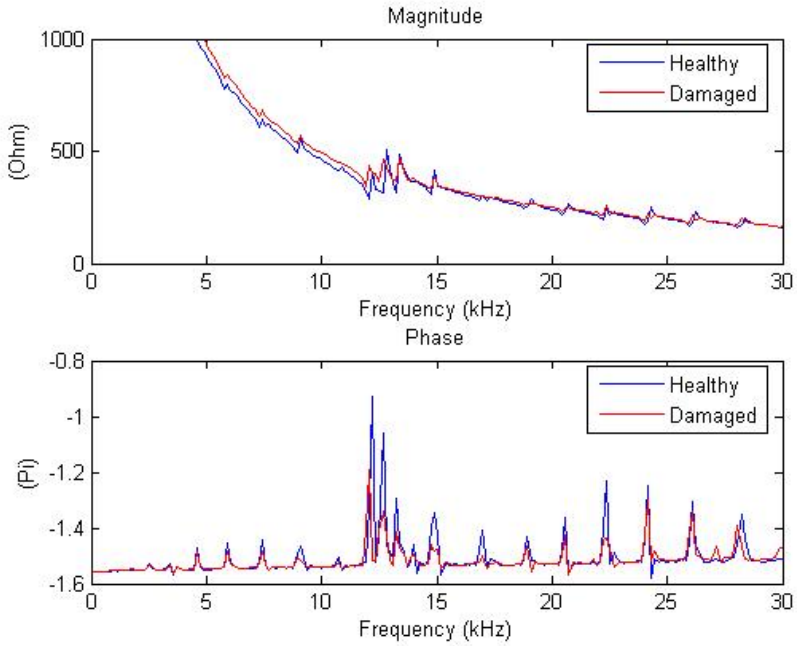

(b) Magnitude and Phase

Figure 3.3: Impedance Profiles of the Healthy and the Damaged Structures

3.3.2 Impedance Profiles for the Temperature Range

The impedance profiles of the baseline and the damaged structures obtained by our SHM system at room temperature (20°C) are shown in Figure 3.4. The impedance profile of a healthy structure is noticeably different from that of a damaged one, which indicates the phase measurement adopted for our system is effective. The damage metric of the damaged structure is obtained as 62 for the damage, which is much greater than the threshold value 27.

It is interesting to note that the profiles show the target frequency range also contains many peaks. Note that the phase of the impedance is zero degree at the resonant frequency if the impedance has only one resonant frequency. Since our structures have multiple peaks as shown in Figure 3.4, the phase is not necessarily zero degree at a peak.

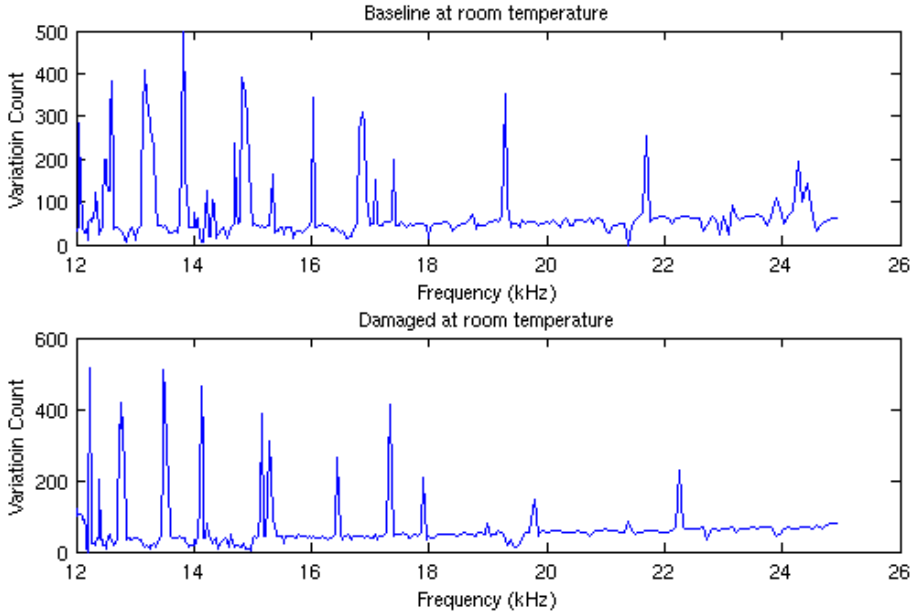

Figure 3.4: Impedance Profiles of the Healthy and the Damaged Structures

3.3.3 Temperature Effect on Impedance Profiles

We examined the effect of the temperature on impedance profiles for our test structures. We obtained baseline impedance profiles at three different temperatures, 0°C, 30°C and 60°C through three repeated experiments, at least a day apart between two

consecutive experiments. Figure 3.5 shows baseline phase profiles for three different temperatures, and each profile is the average value of the three experiments. It is apparent that a profile shifts toward a lower frequency as the temperature increases, but the rate of the shift is not uniform. For example, the peak occurred at 13.27 KHz at temperature 0°C shifts down by 46 Hz as the temperature increases by 30°C, but by 59 Hz for the next 30°C increase. Also, most peaks shrink as temperature increases, but some peaks do not follow the trend.

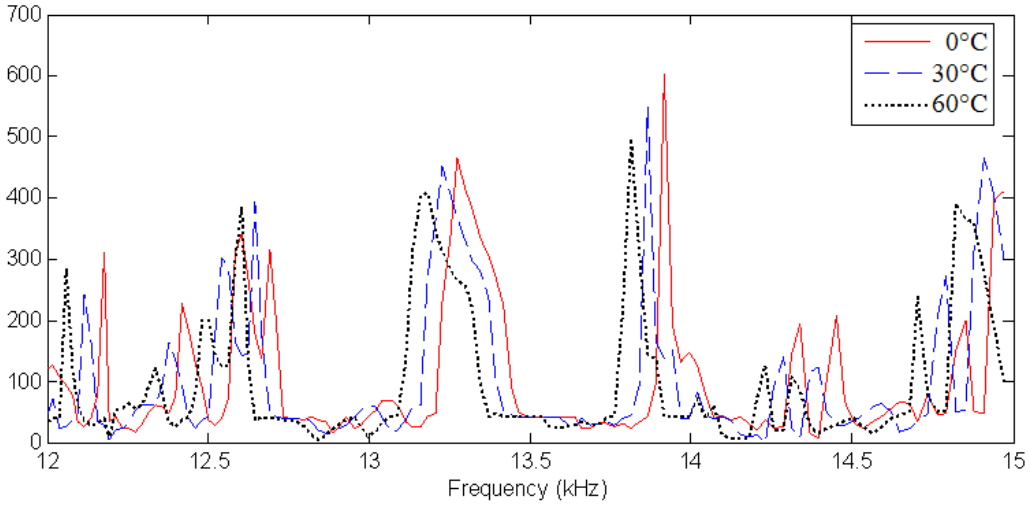

Figure 3.5: Temperature Effect of the Baseline Profile

3.3.4 Necessity for Temperature Compensation of Baseline Profiles

As expected, the impedance profiles of the damaged structure show the same tendency as baseline profiles. The two impedance profiles in Figure 3.6, the baseline profile at 10°C and the profile of the damaged one at 70°C, are very close. The damage metric falls below the threshold for our SHM system to fail the detection. However, the damage is detected under the baseline profile obtained at 70°C. It illustrates that use of one baseline profile without proper temperature compensation fails detection of some damages. It means that an SHM system requires sensing the ambient temperature.

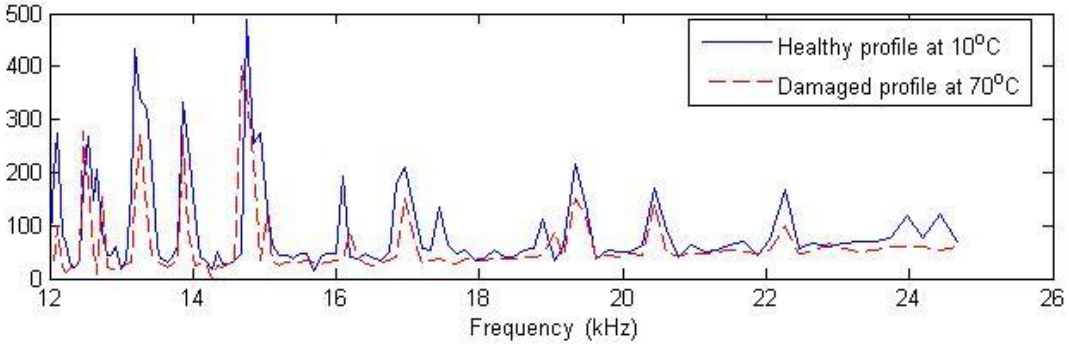

Figure 3.6: The Profiles of Baseline at 10°C and the Damaged Structure at 70°C

3.4 Compensation of Temperature Effect

Shift of a baseline profile due to the change of the ambient temperature can cause false alarms or missed detections. A straightforward solution is to obtain and pre-store the baseline profile for each possible temperature point of the target temperature range and to use the baseline profile corresponding to the current ambient temperature. However, the scheme requires a large memory increasing the cost of a SHM system. We present a scheme to address the problem, which is based on selection of representative baseline profiles.

3.4.1 Selection of Representative Baseline Profiles

Our approach is to select a small number of representative baseline profiles, from which the profile of a temperature can be estimated. A baseline profile is a nonlinear function of the temperature, which makes it not effective to select baseline profiles at a uniform temperature interval. We propose selection of profiles based on the correlation of profiles for adjacent temperature points. The correlation coefficient ρ_{ij} of two impedance profiles $\phi_i(f)$ at temperature i and $\phi_j(f)$ at temperature j is defined as follows:

$$\rho_{ij} = \sqrt{\frac{\left[\sum_{f=f_1}^{f_2} \phi_i(f)\phi_j(f)\right]^2}{\sum_{f=f_1}^{f_2} \phi_i^{\,2}(f) \sum_{f=f_1}^{f_2} \phi_j^{\,2}(f)}} \qquad (3.1)$$

A high correlation coefficient ρ_{ij} implies that the two impedance profiles at temperature *i* and temperature *j* are strongly correlated, so we can store only one of the two profiles. Further, the profile at a temperature residing between the two temperatures can be estimated with a reasonable accuracy through a linear interpolation.

Table 3-1 shows correlation coefficients of baseline profiles for temperatures from -40°C to 80°C with increment of 10°C. As expected, the correlation coefficient of two baseline profiles decreases as the difference between the two corresponding temperatures increases. However, the rate of the change from a pair of adjacent temperatures to the next pair is not uniform.

Table 3-1: Correlation Coefficients of Baseline Profiles

ρ_{ij}	-40°C	-30°C	-20°C	-10°C	0°C	10°C	20°C	30°C	40°C	50°C	60°C	70°C	80°C
-40°C	1	0.75	0.52	0.37	0.30	0.27	0.20	0.11	0.01	-0.04	-0.07	-0.05	-0.06
-30°C	0.75	1	0.75	0.49	0.39	0.25	0.19	0.18	0.09	0.02	-0.05	-0.06	-0.10
-20°C	0.52	0.75	1	0.70	0.55	0.38	0.28	0.25	0.18	0.12	0.00	-0.02	-0.08
-10°C	0.37	0.49	0.70	1	0.73	0.52	0.33	0.23	0.21	0.17	0.05	0.04	-0.05
0 °C	0.30	0.39	0.55	0.73	1	0.73	0.62	0.34	0.23	0.17	0.13	0.07	-0.02
10 °C	0.27	0.25	0.38	0.52	0.73	1	0.77	0.48	0.31	0.18	0.09	0.12	0.05
20 °C	0.20	0.19	0.28	0.33	0.62	0.77	1	0.67	0.47	0.25	0.12	0.14	0.10
30 °C	0.11	0.18	0.25	0.23	0.34	0.48	0.67	1	0.79	0.37	0.18	0.09	0.11
40 °C	0.01	0.09	0.18	0.21	0.23	0.31	0.47	0.79	1	0.63	0.30	0.17	0.11
50 °C	-0.04	0.02	0.12	0.17	0.17	0.18	0.25	0.37	0.63	1	0.52	0.34	0.22
60°C	-0.07	-0.05	0.00	0.05	0.13	0.09	0.12	0.18	0.30	0.52	1	0.65	0.43
70°C	-0.05	-0.06	-0.02	0.04	0.07	0.12	0.14	0.09	0.17	0.34	0.65	1	0.71
80°C	-0.06	-0.10	-0.08	-0.05	-0.02	0.05	0.10	0.11	0.11	0.22	0.43	0.71	1

We select representative profiles as follows. We identify a cluster of temperatures, in which every pair of baseline profiles within the temperature cluster has the correlation coefficient greater than or equal to 0.6. Then, we select one representative temperature from the cluster and remove all the other temperatures in the cluster from the list. In this way, we identify another cluster for the remaining temperatures and repeat the same process until all the temperature points are included.

Figure 3.7 shows such clusters used for our temperature selection, and the seven selected temperatures out of 13 temperatures are -40°C, -20°C, 10°C, 30°C, 50°C, 60°C

and 70°C. It can be observed that low temperatures are sparsely selected, while the higher temperatures are more densely selected. This effect implies that baseline profiles are more sensitive to high temperatures. The memory saved by saving only seven baseline profiles out of 13 profiles is about 45 %.

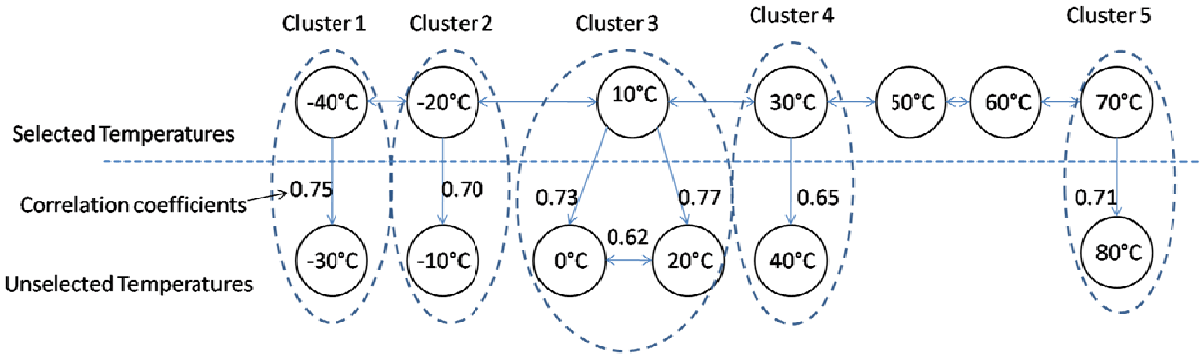

Figure 3.7: Cluster of Temperatures with High Correlation Coefficients

3.4.2 Estimation of Baseline Profiles

As observed in Section 3, a temperature change causes shift in both frequency and magnitude of a profile. We propose estimation of a profile for a given temperature using a linear interpolation between its neighboring selected temperatures as shown in Figure 3.8.

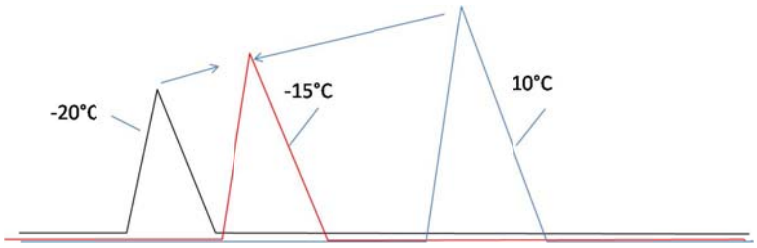

Figure3.8: Linear interpolation of baseline profiles

Assume the current temperature is t_x, while its neighboring selected temperatures are t_1 and t_2 such that $t_1 < t_x < t_2$. The following steps are used to estimate the profile at temperature t_x.

Step1. The profile of t_1 shifts toward a low frequency as t_1 increases toward t_2. Obtain the total amount of the frequency shift Δf from t_1 to t_2. Δf is obtained as the

frequency shift maximizing the correlation between the shifted profile of t_1 and the profile of t_2.

Step2. Calculate the amount of the frequency shift from temperature t_1 and from t_2 to the target temperature t_x by dividing the total frequency shift Δf in proportion to its relative distance. The frequency shifts are

$$\Delta f_1 = \frac{t_x - t_1}{t_2 - t_1}\Delta f \quad , \quad \Delta f_2 = \frac{t_2 - t_x}{t_2 - t_1}\Delta f \quad . \tag{3.2}$$

Then, the shifted profiles $\phi_{1tox}(f)$ and $\phi_{2tox}(f)$ can be represented as follows:

$$\phi_{1tox}(f) = \phi_1(f + \Delta f_1) \quad , \quad \phi_{2tox}(f) = \phi_2(f - \Delta f_2) \quad . \tag{3.3}$$

Step3. Calculate the profile of $\mathrm{t_x}$ with a linear weight on $\phi_{1tox}(f)$ and $\phi_{2tox}(f)$ as follows:

$$\phi_x(f) = \frac{t_2 - t_x}{t_2 - t_1}\phi_{1tox}(f) + \frac{t_x - t_1}{t_2 - t_1}\phi_{2tox}(f) \tag{3.4}$$

3.4.3 Effectiveness of the Proposed Profile Estimation Method

We checked the effectiveness of our estimation method for two temperatures, -15°C and 35°C. The baseline profile at -15°C was constructed from the two baseline profiles of temperatures at -20°C and 10°C using the estimation method, and the constructed baseline profile is compared against a measured one at the temperature -15°C. The baseline profile at 35°C was constructed from the two baselines of temperatures at 30°C and 50°C. Figure 3.9 shows the two estimated profiles against their measured counterparts, and estimated and measured ones match nearly perfectly for both temperatures.

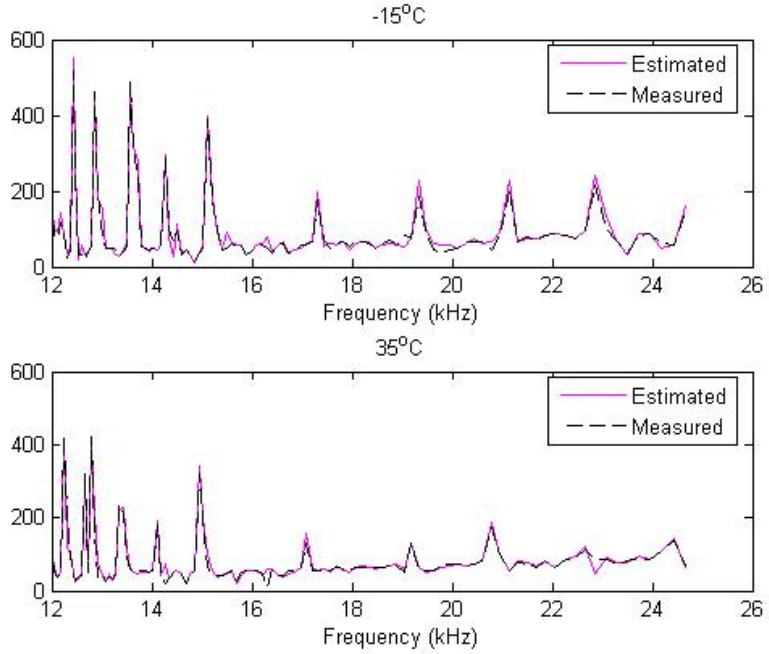

Figure3.9: Estimated and Measured Baseline Profiles at Temperatures at -15°C and 35°C

In order to quantify the effectiveness, we examined the damage metrics of the profiles for the two temperatures. As noted in Section 2.2, the damage metric is obtained as the normalized absolute sum of difference between the baseline and the structure-under-test (SUT) profiles. The SUT profiles for this case are impedance profiles of the healthy structure at temperatures of -15 °C and 35 °C. The threshold value is set to 3σ, where σ is the variation of the baseline profiles for four repeated experiments at the room temperature of 20°C. The threshold value was obtained as 27 from the experiments.

We considered three different baseline profiles. The first baseline profile is the measured one obtained at the room temperature of 20°C. The DMs for temperatures at -15°C and 35°C are shown in the second column of Table 3-2. The DMs for both temperatures, 58 and 44, exceed the threshold value of 27. This means that the structure under test is considered as damaged at both temperatures due to the variations of the profiles caused by the temperature changes. The second case considers the measured baseline profiles of selected neighbor temperatures. Specifically, the profile of temperature -10°C is for the temperature -15°C case and the profile of 30°C is for the

temperature 35°C case. The DMs for this case are shown in the next column of the table. The DMs are decreased compared with the first case, but they are in the vicinity of the threshold value to cause possible false alarms. The final case is that the baseline profiles are those estimated through the proposed scheme. The DMs are well below the threshold value, so that no false alarm will occur. We should restate that the structure under test is the healthy one for all the three cases.

Table 3-2: Damage Metric for Different Baseline Profiles

Baseline	Baseline at Room Temperature (20°C)	Baselines at -20°C	Baselines at 30°C	Estimated Baselines
-15°C	58	31	-	10
35°C	44	-	25	7

3.5 Conclusion

An impedance based SHM system employs a piezoelectric patch to excite the structure under test and capture its response. Impedance-based SHM offers several advantages over other methods such as good performance for local damage detection and simple hardware. A major problem for impedance-based SHM is temperature dependency. Specifically, baseline impedance profiles of structures vary as the ambient temperature changes. In this chapter, we proposed a new method to compensate the affect of temperature on baseline profiles. Our method is to select a small subset of baseline profiles for some critical temperatures and estimates the baseline profile for a given ambient temperature through interpolation. We incorporated our method into our digital SHM system and investigated the effectiveness of our method. Our experimental results show that (i) our method reduces the number of baseline profiles to be stored, and (ii) estimates the baseline profile of a give temperature accurately.

References

[1] G. Park, K. Kabeya, H. H. Cudney, and D. J. Inman, "Impedance-based structural health monitoring for temperature varying applications," JSME International Journal, Series A, 42, 249-258 (1999)

[2] K. Krishnamurthy, F. Lalande, and C. A. Rogers, "Effects of temperature on the electrical impedance of piezoelectric sensors," Proc. SPIE 2717,302-310 (1996)

[3] J. Kim, B. L. Grisso, D. S. Ha, and D. J. Inman, "An all-digital low-power structural health monitoring system,", IEEE Conference on Technologies for Homeland Security,123-8 (2007)

[4] G. Park, S. Hoon, C. R. Farrar, and D. J. Inman, "Overview of piezoelectric impedance-based health monitoring and path forward," The Shock and Vibration Digest 35, 451-463 (2003)

[5] J. Kim, "Low-Power System Design for Impedance-Based Structural Health Monitoring", PhD Thesis, Virginia Polytechnic Institute and State University (2007)

[6] J. Kim, B. L. Grisso, D. S. Ha, and D. J. Inman, "Digital wideband excitation technique for impedance-based structural health monitoring systems," IEEE International Symposium on Circuits and Systems, 4 (2007).

[7] J. Kim, B. L. Grisso, D. S. Ha, and D. J. Inman, "A system-on-board approach for impedance-based structural health monitoring," Proc. SPIE 6529 PART 1 , 65290 (2007)

[8] F. Sun, C. Liang and C. A. Rogers. "Structural frequency response function acquisition via electric impedance measurement of surface bonded piezoelectric sensor/actuator" Proc. AIAA/ASME/ASCE/AHS/ASC 36th Structure, Structural Dynamics and Materials Conference, 3450-3458 (1995)

[9] G. Park, H. H. Cudney, and D. J. Inman, "Impedance-based health monitoring technique for massive structures and high-temperature structures," Proc. SPIE 3670, 461-9 (1999)

[10] D. M. Peairs, P. A. Tarazaga, and D. J. Inman, "Frequency range selection for impedance-based structural health monitoring," Transactions of the ASME. Journal of

Vibration and Acoustics, vol. 129, 701-9 (2007)
[11] S. Park, Y. Chung-Bang, D. J. Inman, and P. Gyuhae, "Wireless structural health monitoring for critical members of civil infrastructures using piezoelectric active sensors," Proc. SPIE 6935, 69350-1 (2008)
[12] C. E. Woon and L. D. Mitchell, "Temperature-induced variations in structural dynamic characteristics. I. Experimental," Proc. SPIE 2868, 263-74 (1996)
[13] C. E. Woon and L. D. Mitchell, "Temperature-induced variations in structural dynamic characteristics. II. Analytical," Proc. SPIE 2868, 58-70 (1996)

Chapter 4: Conclusion

Impedance-base Structural Health Monitoring is an effective method for local damage detection. However, high installation and maintenance cost and sensitivity to ambient environment block the method to be widely deployed in real-world applications. Development of low power wireless sensors and employment of temperature compensation algorithm are possible solutions to the problems above.

We presented a low-power wireless autonomous SHM node ASN-2 in Chapter 2. We incorporated three methods to save power. First, entire data processing is performed on board, which minimizes radio transmission time. Considering the radio of a wireless sensor node consumes the most power, reduction of transmission time saves substantial power. Second, a rectangular pulse train is used to excite a PZT patch instead of a sinusoidal wave. It eliminates a DAC and reduces memory space. Third, it senses the phase of the response signal instead of the magnitude. Sensing the phase of the signal eliminates an ADC and FFT operation, which not only saves power but enables us to use a low-end low-power processor. Our SHM sensor node ASN-2 is implemented using a TI MSP430 microcontroller evaluation board. A cluster of ASN-2 nodes forms a wireless network. Each node wakes up at a predetermined interval such as once in four hours, performs a SHM operation, reports the result to the host computer wirelessly, and sleeps back. The power consumption of our ASN-2 is 0.15 mW during the inactive mode and 18 mW during the active mode. Each SHM operation takes about 13 seconds to consume 236 mJ. When our ASN-2 operates once in every four hours, it can run for about 2.5 years with two AAA-size batteries.

In Chapter 3, we proposed a new method to compensate the effect of temperature on baseline profiles. Our method is to select a small subset of baseline profiles for some critical temperatures and estimates the baseline profile for a given ambient temperature through interpolation. We incorporated our method into our SHM system and

investigated the effectiveness of our method. Our experimental results show that our method reduces the number of baseline profiles to be stored by 45%, and estimates the baseline profile of a given temperature accurately.

With the contribution of the above two approaches, the application of impedance-based SHM is widely expanded. Low power wireless sensors are suitable for civil and industrial structures where cable connection is not accessible or where replacement of power source is expensive. Moreover, with temperature compensation, impedance-based method is more flexible to be distributed in the environment where temperature variation is a critical issue.

Many research topics related to improvement of SHM sensor development are open for consideration. Some of the possible issues are:

a. Ambient energy sources, such as solar, wind, vibration, thermal difference are available to power SHM sensor. How to harvest this energy efficiently is an interesting topic. With sufficient energy harvested form ambient sources, it is possible to develop SHM sensors for which power consumption is no longer a limitation of operation life time.

b. Instead of using general microcontrollers, design an Application Specific Integrated Circuit (ASIC) will further reduce the power consumption, which in return, will make the objective of energy harvesting easier to approach

c. Star formed topology can be extended to mesh, multi-hop and other forms depending on the in situ environment. Also properly designed communication protocol in higher layers may further reduce transmission power of the whole network.

d. More efficient algorithms can be considered to compensate environmental variations if system complexity is not a major concern.

The challenges in this field are not limited as above. More practical issues may appear in real-world applications. However, the work presented in this thesis will serve as an important reference for future work.